

Determination of the focused beam waist of lasers with weak measurements

Linguo Xie (谢林果)¹, Xiaodong Qiu (邱晓东)¹, Jiangdong Qiu (邱疆冬)¹, Zhiyou Zhang (张志友)^{1,2,*}, Jinglei Du (杜惊雷)^{1,2}, and Fuhua Gao (高福华)^{1,2}

¹Key Laboratory of High Energy Density Physics and Technology of Ministry of Education, Sichuan University, Chengdu 610064, China

²College of Physical Science and Technology, Sichuan University, Chengdu 610064, China

*Corresponding author: zhangzhiyou@scu.edu.cn

Received August 5, 2015; accepted September 18, 2015; posted online October 14, 2015

In this Letter, a method for detecting the focused beam waist of lasers is proposed by using weak measurements based on the so-called weak-value amplification. We establish a propagation model to describe the quantitative relation between the beam waist and the amplified shift of the spin Hall effect of light (SHEL), which is sensitive to the variation of the beam waist. We experimentally measure the amplified shift corresponding to a different beam waist and the experimental data agrees well with theoretical calculation. These results confirm the rationality and feasibility of our method.

OCIS codes: 240.3695, 260.5430, 140.3295.

doi: 10.3788/COL201513.112401.

The accurate measurement of the focused beam waist of lasers is necessary in many applications, such as the Z scan method^[1], thermal lens spectrometry^[2,3], laser micro-nano processing^[4], and optical tweezers^[5,6]. Many techniques have been developed to measure the beam waist; for instance, the knife-edge technique^[7], the pinhole method^[8], the ronchi ruling method^[9], and slit scan^[10]. However, the direct measuring accuracy of those methods mentioned above is insufficient with the rapid development of laser fabrication and measuring technologies in recent years. There is an urgent need to improve the measuring accuracy of the focused beam waist.

Recently, weak measurements^[11] based on the post-selection weak-value amplification have drawn increasing attention due to its important applications in precision metrology^[12-17]. One of the typical scenarios is observation of the optical polarization-dependent effect, so-called the spin Hall effect of light (SHEL), via weak measurements^[12,18]. The SHEL manifests itself as opposite transverse displacements of two circularly polarized components of a linearly polarized light beam reflected or refracted at an interface between two materials. Generally, the SHEL is considered as a result of the Berry geometric phase corresponding to the spin-orbit coupling^[12,19,20]. The interesting point is that, with the aid of SHEL, weak measurements can be used to determine many other unknown parameters, such as position of nanoparticles^[21], chirality of light^[22], graphene layers^[23], thickness of the metal film^[24], and even magneto-optical constant of Fe films^[25]. In this work, weak measurements are employed to determine the focused beam waist of lasers with the aid of SHEL.

We first establish an angular spectrum model to simultaneously describe the SHEL and weak measurements in detail. The coordinate systems are shown in Fig. 1; two beam coordinate systems ($x_{i,r}$, $y_{i,r}$, $z_{i,r}$) attach to the

incident and reflected light beams, respectively. The Z axis of the laboratory coordinate system (X , Y , Z) is perpendicular to the reflection surface ($Z = 0$). Consider the incident Gaussian light beam with a horizontal polarization state, its angular spectrum can be expressed as in the incident beam coordinate system as

$$\tilde{E}_i^H = \frac{\omega_0}{\sqrt{2\pi}} \exp\left[-\frac{\omega_0^2(k_{ix}^2 + k_{iy}^2)}{4}\right] \vec{e}_{ix}, \quad (1)$$

where ω_0 is the focused beam waist. Moreover, we note that the horizontal incident polarization state can be regarded as the preselection process of weak measurements. By introducing the boundary conditions, the reflected angular spectrum can be obtained with the relation^[26]

$$\begin{bmatrix} \tilde{E}_r^H \\ \tilde{E}_r^V \end{bmatrix} = \begin{bmatrix} r_p & \frac{k_{ry}(r_p+r_s)\cot\theta_i}{k_0} \\ -\frac{k_{ry}(r_p+r_s)\cot\theta_i}{k_0} & r_s \end{bmatrix} \begin{bmatrix} \tilde{E}_i^H \\ \tilde{E}_i^V \end{bmatrix}, \quad (2)$$

where θ_i denotes the incident angle, r_p and r_s are the Fresnel reflection coefficients, and $k_0 = 2\pi/\lambda$ with λ being the wavelength of light in air. In the spin basis, we have $\tilde{E}_{r(\sigma)} = (\tilde{E}_r^H + i\sigma\tilde{E}_r^V)/\sqrt{2}$, $\sigma = \pm 1$ represents the left and right circular polarization (spin components), respectively. Equation (1), together with Eq. (2), the reflected angular spectrums of the spin components, can be written as

$$\tilde{E}_{r(\sigma)} = \frac{\omega_0 r_p}{2\sqrt{\pi}} \exp\left[-\frac{\omega_0^2(k_{rx}^2 + k_{ry}^2)}{4}\right] \exp(i\sigma k_{ry}\delta), \quad (3)$$

where $\exp(i\sigma k_{ry}\delta)$ represents the spin-orbit interaction that results in the SHEL and $\delta = (1 + r_s/r_p)\cot\theta_i/k_0$

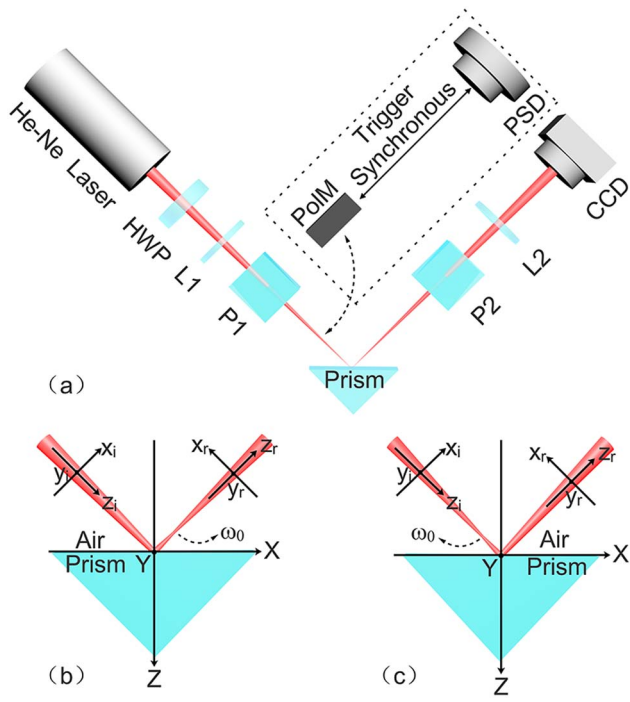


Fig. 1. (a) Experimental setup: the light source is a He-Ne laser at 632.8 nm (Thorlabs HNL210L); HWP, half-wave plate for attenuating the light intensity; L1, short-focus lens (variable); P1 and P2, Glan polarizers; prism with refractive index $n = 1.515$ (at 632.8 nm); L2, long-focus lens (150 mm); CCD, Coherent LaserCam HR. Dotted box: the schematic of the standard lock-in technology. PolM, polarization modulator; PSD, position sensitive detector; their frequencies keep synchronous. (b) and (c) denote the focused beam waist at different positions relative to the reflection surface.

denotes the coupling strength. In addition, we note that the spin-orbit interaction allows for the weak coupling process between the observable (spin operator) and the meter (transverse distribution of the reflected light beam) of weak measurements. By using the Fourier transform we can get the expression of the reflected light field

$$E_{r|\sigma} = \iint \tilde{E}_{r|\sigma} \exp[i(k_{rx}x_r + k_{ry}y_r + k_{rz}z_r)] dk_{rx} dk_{ry}, \quad (4)$$

where $k_{rz} = \sqrt{k_r^2 - k_{rx}^2 - k_{ry}^2}$ is the central wave vector and $k_r = k_0$. Now, the transverse displacements of the spin components induced by the SHEL can be calculated with geometric prediction

$$\delta_{r|\sigma} = \frac{\iint y_r I_{r|\sigma} dx_r dy_r}{\iint I_{r|\sigma} dx_r dy_r}, \quad (5)$$

where $I_{r|\sigma}$ denotes the intensity distribution of the spin components.

To detect the tiny transverse displacement induced by the SHEL, weak measurements is employed. As it is well

known^[11,12], weak measurements can be divided into three stages. First, preselection of the system; second, weak coupling between the observable and the meter; third, post-selection of the information of the system. Now, weak measurements can be accomplished with the final step and the postselection state can be written as

$$\tilde{E}_{\text{post}} = \tilde{E}_r^H \sin \Delta + \tilde{E}_r^V \cos \Delta, \quad (6)$$

where \tilde{E}_r^H and \tilde{E}_r^V are obtained from Eq. (2) and Δ denotes the postselection angle. When $\Delta \ll 1$, we can obtain a large pure imaginary weak value. For an imaginary weak value, the propagation amplification F should be introduced to modify the amplification factor of weak measurements, i.e., so-called modified weak value^[12]. In addition, we note that the propagation amplification is closely related to the beam waist ($F = \lambda z_r / \pi \omega_0^2$, where z_r denotes the free propagation distance)^[12,27,28]. After the Fourier transform and integral calculation (similar to Eqs. (4) and (5)), we get the analytic expression of amplified shift

$$\Delta_H = \frac{2z_r \delta_r \tan \Delta}{\delta_r^2 k_0 + 2R_0 \tan^2 \Delta}, \quad (7)$$

where $R_0 = k_0 \omega_0^2 / 2$ is the Rayleigh length after L1. Therefore, the amplified shift is associated with the beam waist. This is why the beam waist can be determined by weak measurements. Furthermore, we find that Eq. (7) can be simplified to be consistent with the results in Ref. [12] when $|\Delta| \gg |\delta_r / \omega_0|$ (i.e., the left term of the denominator can be ignored).

By using $\partial \Delta_H / \partial \omega_0$, we investigate the dependence of the amplified shift on the beam waist. As shown in Fig. 2, the amplified shift shows different sensitivities to the beam waist at different incident and postselection angles, and the greatest sensitivity can be obtained in these conditions according to the black dashed lines. Note that greater sensitivity means higher measuring accuracy can be obtained in the experiments.

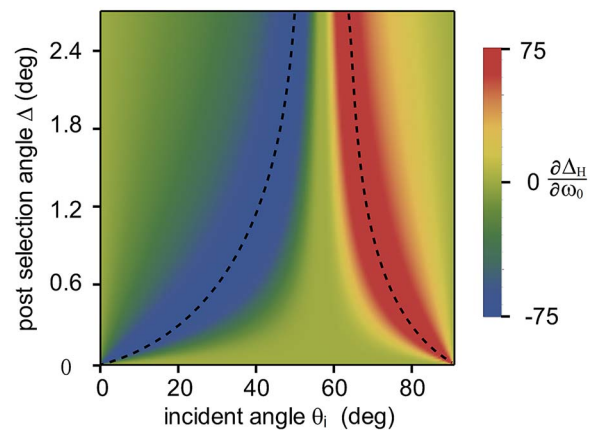


Fig. 2. $\partial \Delta_H / \partial \omega_0$ (the sensitivity of the amplified shift to the beam waist) varies with incident and postselection angles. The extreme values are indicated by the black dashed lines.

The experimental setup is shown in Fig. 1(a). A Gaussian light beam generated by the He-Ne laser passes through a half-wave plate (HWP) and then is focused by the first lens (L1). Here, we obtain the focused light beams with different beam waist ω_0 by adjusting the focal length of L1. The first Glan polarizer (P1) is used to control the incident polarization state (i.e., preselection). Upon reflection at the surface of BK7 prism, the SHEL takes place. The postselection state is obtained after the second Glan polarizer (P2). Finally, the intensity barycenter shift of the light beam collimated by the second lens (L2) is recorded by the CCD.

In our experiment, the focal length of L1 is chosen as 30.0, 35.0, and 38.1 mm. Based on the imaging principle, the focused beam waists can be obtained with the relation

$$\omega_0 = \frac{f \omega}{\sqrt{R^2 + (d - f^2)}}, \quad (8)$$

where f is the focal length of L1, $R = k_0 \omega^2 / 2$ is the initial Rayleigh distance with $\omega = 0.35$ mm being the initial beam waist of lasers, and the transmission distance $d = 240$ or 280 mm is controlled in the experiment. The corresponding beam waists of the focused light beam are 15.96, 19.09, and 20.81 μm . According to the previous analysis of Fig. 2, the incident angle is chosen as 65° and we measure the amplified shift changing with the postselection angle every 0.04° from 1.2° to 1.8° .

Figure 3 shows the amplified shift changing with the postselection angle for different beam waists. The dots denote the experimental data obtained with weak measurements and the curves represent the theoretical calculation results by using the beam waist mentioned above. It is easy to find that the amplified shifts corresponding to different beam waists show great difference with each

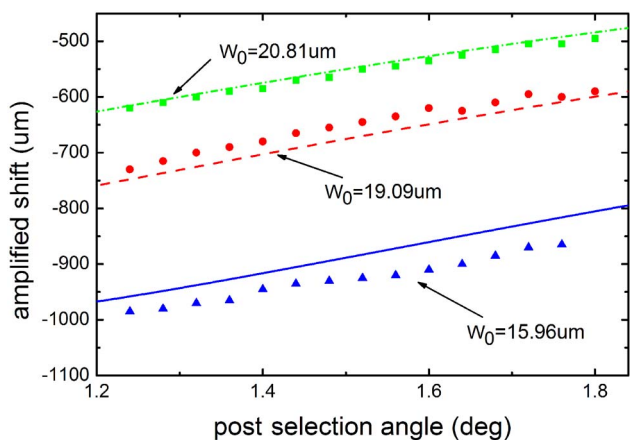


Fig. 3. Amplified shift changing with the postselection angle and the beam waist. Here, the beam waist is chosen as 15.96, 19.09, and 20.81 μm . The incident angle is 65° . The squares, circles, and triangles denote the experiment data corresponding to different beam waists. The curves are theoretical predictions from Eq. (7).

other. In addition, the experimental results are in agreement with the theoretical prediction. According to Eq. (7), the focused beam waist can be expressed with the amplified shift

$$\omega_0 = \sqrt{\left(\frac{2z_r}{k_0 \Delta_H} - \frac{\delta_r}{\tan \Delta}\right) \frac{\delta_r}{\tan \Delta}}. \quad (9)$$

The average values of the focused beam waist are obtained with 15.48, 19.62, and 20.66 μm by using the measured values of the amplified shift. We note that the discrepancy is mainly caused by misalignment of the experimental setup. These results confirm the rationality and feasibility of the method to determine the beam waist with weak measurements.

Obviously, the measuring accuracy of our method depends on two points. First, the sensitivity of the amplified shift to the beam waist; second, the measuring accuracy of the amplified shift. From both Figs. 2 and 3 we can find the greatest sensitivity of the amplified shift to the beam waist $\partial \Delta_H / \partial \omega_0 \approx 75$. Moreover, the measuring error of the amplified shift is less than 3 μm (here, the error caused by the misalignment of the experimental setup is not taken into account). Therefore, we can obtain a measuring accuracy of the beam waist, achieving up to 0.04 μm via weak measurements. Furthermore, with respect to the conventional method as shown in Figs. 1(b) and 1(c), our method has an advantage that we do not need to determine the position of the beam waist in the measurement since the amplified shift is not influenced by the position of the beam waist^[12]. We note that the in-plane spin splitting^[27,29] that is sensitive to the focused beam waist can also be applied to determine the beam waist.

In addition, as shown in Fig. 1(a), the standard lock-in technology^[30,31] can be introduced to improve the measuring accuracy. A polarization modulator (PolM) is added after P1 (the incident polarization state can be switched between horizontal and vertical polarization at a fixed frequency) and the CCD is replaced by a position sensitive detector (PSD) whose frequency keeps synchronous with the PolM. Based on our theory, the amplified shift for the vertical polarization $\Delta_V \rightarrow 0$ can be regarded as the reference signal. Therefore, the measuring accuracy of the beam waist can be increased by orders of magnitude since the position resolution is ≈ 20 nm for the PSD^[31].

In conclusion, a propagation model is established to reveal the quantitative relation between the focused beam waist and the amplified shift of the SHEL. We find that the amplified shift is sensitive to the variation of the beam waist. The amplified shift corresponding to different beam waists is detected with weak measurements and the experimental results agree well with our theoretical prediction. In addition, we theoretically propose that the measuring accuracy can be improved by orders of magnitude by combining the standard lock-in technology. Our research provides an effective method to determine the focused beam waist of lasers, which is of great significance for

precision laser measurements and super-resolution optical microscopes.

This work was supported by the National Natural Science Foundation of China under Grant Nos. 11305111 and 61377054.

References

1. F. Z. Henari, K. Cazzini, F. E. Akkari, and J. B. Werner, *J. Appl. Phys.* **78**, 1373 (1995).
2. M. L. Baesso, J. Shen, and R. D. Snook, *J. Appl. Phys.* **75**, 3732 (1994).
3. K. A. Ghaleb and J. Georges, *Appl. Spectrosc.* **58**, 1116 (2004).
4. S. Nikumb, Q. Chen, C. Li, H. Reshef, H. Zheng, H. Qiu, and D. Low, *Thin Solid Films* **477**, 216 (2005).
5. M. Zhong, X. Wang, J. Zhou, Z. Wang, and Y. Li, *Chin. Opt. Lett.* **12**, 011403 (2014).
6. J. Yu, X. Tong, C. Li, Y. Huang, and A. Ye, *Chin. Opt. Lett.* **11**, 091701 (2013).
7. J. Arnaud, W. Hubbarb, G. Mandeville, B. D. Claviere, E. Franke, and J. Franke, *Appl. Opt.* **10**, 2775 (1971).
8. P. Shayler, *Appl. Opt.* **17**, 2673 (1978).
9. D. Cohen, B. Little, and F. Luecke, *Appl. Opt.* **23**, 637 (1984).
10. P. B. Chapple, *Opt. Eng.* **33**, 2461 (1994).
11. Y. Aharonov, D. Z. Albert, and L. Vaidman, *Phys. Rev. Lett.* **60**, 1351 (1988).
12. O. Hosten and P. Kwiat, *Science* **319**, 787 (2008).
13. P. B. Dixon, D. J. Starling, A. N. Jordan, and J. C. Howell, *Phys. Rev. Lett.* **102**, 173601 (2009).
14. N. Brunner and C. Simon, *Phys. Rev. Lett.* **105**, 010405 (2010).
15. D. J. Starling, P. B. Dixon, N. S. Williams, A. N. Jordan, and J. C. Howell, *Phys. Rev. A* **82**, 011802 (2010).
16. X. Xu, Y. Kedem, K. Sun, L. Vaidman, C. Li, and G. Guo, *Phys. Rev. Lett.* **111**, 033604 (2013).
17. L. J. Salazar-Serrano, D. Janner, N. Brunner, V. Pruneri, and J. P. Torres, *Phys. Rev. A* **89**, 012126 (2014).
18. Y. Qin, Y. Li, H. He, and Q. Gong, *Opt. Lett.* **34**, 2551 (2009).
19. M. Onoda, S. Murakami, and N. Nagaosa, *Phys. Rev. Lett.* **93**, 083901 (2004).
20. K. Y. Bliokh and Y. P. Bliokh, *Phys. Rev. Lett.* **96**, 073903 (2006).
21. O. G. Rodríguez-Herrera, D. Lara, K. Y. Bliokh, E. A. Ostrovskaya, and C. Dainty, *Phys. Rev. Lett.* **104**, 253601 (2010).
22. Y. Gorodetski, K. Y. Bliokh, B. Stein, C. Genet, N. Shitrit, V. Kleiner, E. Hasman, and T. W. Ebbesen, *Phys. Rev. Lett.* **109**, 013901 (2012).
23. X. Zhou, X. Ling, H. Luo, and S. Wen, *Appl. Phys. Lett.* **101**, 251602 (2012).
24. X. Zhou, Z. Xiao, H. Luo, and S. Wen, *Phys. Rev. A* **85**, 043809 (2012).
25. X. Qiu, X. Zhou, D. Hu, J. Du, F. Gao, Z. Zhang, and H. Luo, *Appl. Phys. Lett.* **105**, 131111 (2014).
26. H. Luo, X. Zhou, W. Shu, S. Wen, and D. Fan, *Phys. Rev. A* **84**, 043806 (2011).
27. X. Qiu, Z. Zhang, L. Xie, J. Qiu, F. Gao, and J. Du, *Opt. Lett.* **40**, 1018 (2015).
28. X. Qiu, L. Xie, J. Qiu, Z. Zhang, J. Du, and F. Gao, *Opt. Express* **23**, 018823 (2015).
29. X. Zhou, H. Luo, and S. Wen, *Opt. Express* **20**, 016003 (2012).
30. H. Gilles, S. Girard, and J. Hamel, *Opt. Lett.* **27**, 1421 (2002).
31. X. Yin and L. Hesselink, *Appl. Phys. Lett.* **89**, 261108 (2006).